Published in final edited form as:
Biol Psychol. 2012 February ; 89(2): 450–459. doi:10.1016/j.biopsycho.2011.12.012.

Resting cerebral metabolism correlates with skin conductance and functional brain activation during fear conditioning

Clas Linnman[1], **Mohamed A. Zeidan**[1], **Roger K Pitman**[1], and **Mohammed R. Milad**[1]
[1]Department of Psychiatry, Harvard Medical School & Massachusetts General Hospital, Charlestown, MA, USA

Abstract

We investigated whether resting brain metabolism can be used to predict autonomic and neuronal responses during fear conditioning in 20 healthy humans. Regional cerebral metabolic rate for glucose was measured via positron emission tomography at rest. During conditioning, autonomic responses were measured via skin conductance, and blood oxygen level dependent signal was measured via functional magnetic resonance imaging. Resting dorsal anterior cingulate metabolism positively predicted differentially conditioned skin conductance responses. Midbrain and insula resting metabolism negatively predicted midbrain and insula functional reactivity, while dorsal anterior cingulate resting metabolism positively predicted midbrain functional reactivity. We conclude that resting metabolism in limbic areas can predict some aspects of psychophysiological and neuronal reactivity during fear learning.

Introduction

Fear conditioning is an associative learning paradigm whereby an initially neutral stimulus, such as a light, is presented with an aversive unconditioned stimulus (US), such as an electric shock. After such paired presentations, the conditioned stimulus (CS) comes to elicit an acquired fear response in the absence of the US. Human functional magnetic resonance imaging (fMRI) studies of fear conditioning have identified a network that includes the midbrain (periaqueductal gray) in rats (Johansen et al., 2010), amygdala, dorsal anterior cingulate cortex (dACC, sometimes referred to as anterior middle cingulate cortex) and the anterior insula (Linnman et al., 2011; Sehlmeyer et al., 2009). This network is engaged during the acquisition of fear conditioning and in other emotional tasks such as responses to fearful faces (reviewed in Fusar-Poli et al., 2009). In contrast, the ventromedial prefrontal cortex (vmPFC) is involved in extinction learning and dampening of fear(Kalisch et al., 2006; Milad et al., 2007b; Phelps et al., 2004). Variation in these regions has been related to anxiety and mood disorders (Etkin and Wager, 2007; Graham and Milad, 2011; Rauch et al., 2006; Shin and Liberzon, 2010) as well as to vulnerability to anxiety (Indovina et al., 2011).

A clinically relevant question is whether *resting* metabolism in the above conditioned fear acquisition network might predict fear learning and associated neuronal *reactivity* in humans, given that resting brain activity is known to influence behavior (Raichle and Mintun, 2006). Uptake of [^{18}F] 2-fluoro-2-deoxy-d-glucose (FDG), measured via positron emission tomography (PET) provides an estimate of resting regional brain metabolism that

closely correlates with neuronal signaling (Sokoloff, 1977). Functional magnetic resonance imaging (fMRI) provides an indirect measure of neuronal *reactivity* through the blood-oxygen-level-dependent (BOLD) signal (Logothetis, 2002; Ogawa et al., 1990). Elevated resting metabolism in the dACC constitutes a familial risk factor for the development of posttraumatic stress disorder (PTSD) (Shin et al., 2009), and BOLD signal in dACC is related to conditioned fear expression (Milad et al., 2007a). We have recently shown that resting activity of the amygdala, dACC and vmPFC (measured by PET) can predict fear extinction and recall of fear extinction (Linnman et al., in press). Here, we investigated whether regional resting brain *activity* (metabolism) predicts brain *reactivity* (BOLD) to fear conditioning?

We first measured resting regional brain metabolism in healthy individuals using FDG PET. The same subjects subsequently underwent fear conditioning while in a 3T fMRI scanner. We expected fear conditioning to induce skin conductance responses (SCRs) and BOLD activation of the fear-conditioning network (midbrain, amygdala, dACC and anterior insula). We further expected dACC and amygdala reactivity to correlate with SCR magnitude (Furmark et al., 1997; Milad et al., 2007a). Our analysis then focused on two questions: (1) can regional resting metabolism predict the magnitude of autonomic fear responses (measured by skin conductance)? and (2) can resting metabolism in midbrain, amygdala, dACC, anterior insula and/or vmPFC predict the magnitude of BOLD activations during fear acquisition?

We hypothesized that resting metabolism in amygdala and dACC would predict skin conductance fear responses, as has been observed for structural and functional measures in healthy subjects (Furmark et al., 1997; Milad et al., 2007a). Given the literature indicating dACC involvement in fear learning (Linnman et al., 2011; Milad et al., 2007a; Sehlmeyer et al., 2009; Shackman et al., 2011) and vmPFC involvement in controlling fear (Kalisch et al., 2006; Linnman et al., in press; Milad and Rauch, 2007; Milad et al., 2007b; Nili et al., 2010; Phelps and LeDoux, 2005), we hypothesized that elevated resting dACC metabolism would lead to greater — and elevated resting vmPFC metabolism to lesser — fear-induced BOLD signal.

Methods

Subjects

Twenty healthy adults—10 males and 10 females—mean age 26 (standard deviation 5 years) recruited from the local community participated in the experiment. After a complete explanation of the study's procedure, written informed consent was obtained in accordance with the requirements of the Partners Healthcare System Human Research Committee.

PET imaging procedure

After at least six hours fasting, participants received a bolus injection of ^{18}FDG (approximately 200 MBq) in the antecubital fossa and were placed in a dedicated waiting room, where they were instructed to remain sitting quietly without reading or music, but eyes open, in accordance with a nominal resting state. After a 45-min uptake period, each person was positioned in the scanner (HR+ PET camera (CTI; Knoxville, TN)) and the head was aligned in the scanner relative to the canthomeatal line and gently fixated to minimize head movements. Sixty-three contiguous slices of 2.5 mm were acquired over approximately 20 min in 3D mode with a field of view 157.5 mm (whole brain down to medulla). Images were reconstructed using an iterative algorithm to an in-plane resolution of 4.5 mm. Photon attenuation measurements were made with rotating pin sources containing ^{68}Ge. Additional

corrections in the reconstruction process accounted for scattered radiation, random coincidences, and counting losses due to dead time in the camera electronics.

Fear conditioning procedure

Within 5 days after the PET scan (on average 2 days), subjects underwent fear conditioning during fMR imaging. The experiment consisted of four phases: habituation, fear conditioning, fear extinction, and recall of fear extinction. Data from the latter two phases are presented in a separate manuscript (Linnman et al., in press).

A 62.5% partial reinforcement schedule paradigm was used, as previously described (Milad et al., 2009; Milad et al., 2007b). First, the electric shock (US) was individually adjusted for each participant. The shock consisted of a 500 ms electric shock spike train of 1ms spikes delivered at 50Hz to the second and third fingers of the right hand with currents ranging from 0.2 to 4 mA (levels 0.2, 0.4, 0.6, 0.8, 1.1, 1.4, 1.7, 2.0, 2.3, 4.0 mA). Shock level was determined by increasing stimulation levels stepwise until subjects reported the level to be "highly annoying but not painful". If shock levels were too uncomfortable after a step up, subjects could decrease the level to the previous stimulation level.

Prior to habituation subject were instructed: "You will see images, you will not get shocked". During habituation, which was done in the fMRI while collecting EPI data (not reported), all images in the paradigm (context, two CS+ and the CS−) were presented twice with no shock in order to familiarize the subjects with the scan procedure an ensure they could see the images properly.

Prior to the conditioning phase of the experiment, subjects were instructed: "You will see images and you may or may not get shocked. Any pattern that you observe will hold." During fear conditioning, subjects were presented with an image of a room containing an unlit lamp on a desk. The lamp was then switched on to one of three colors (blue, red, or yellow). Two of the colors (CS+s) were followed by an electric shock (US) in 62.5% of the cases, whereas the third color (CS−) was never followed by a shock. The fear conditioning procedure entailed 32 lamp presentations, of which 16 were CS− trials, 10 were trials involving one (5 trials) or the other (5 trials) of the two CS+s followed by a shock, and six were trials involving one or the other of the CS+s not followed by a shock. Between trials, a black screen was displayed with an inter-trial interval of 12 to 18 seconds. The lamp color sequence was counterbalanced across subjects with a pseudo-random presentation order and the two different CS+ stimuli were presented in sequential order (i.e first 8 blue CS+ intermingled with 8 yellow CS− then 8 Red CS+ intermingled with 8 yellow CS−). The very first trial in the conditioning paradigm was always a CS+ trial. The CS duration (6 s) was kept constant across trials so subject could learn to predict when the US would be delivered. The US, delivered immediately after the CS offset. Two different CS+ stimuli were used because we were also interested in the effects of extinction, where one stimulus was extinguished, and the other was not extinguished (see Linnman et al. in press for the fear extinction data). The first CS+ and CS− trials were excluded from all SCR and fMRI analyses, as differential conditioning would not have been acquired in these two trials. SCR and BOLD analysis were conducted on the subsequent 7 CS+ and 7 CS− trials (the remaining second set of CS+ and CS− trials were not included).

Psychophysiological Measures

A Coulbourn Modular Instrument System (Allentown, PA) was used to record skin conductance levels using 8 mm (sensor diameter) Ag/AgCl radiotranslucent electrodes (BioPac Systems Inc., Goleta, CA) placed 14 mm apart on the palm of the participant's left hand. The SCR for each CS trial was calculated by subtracting the mean skin conductance

level 2 sec before CS onset from the highest skin conductance level recorded during the 6 sec CS duration. The SCR responses were square root transformed to be used in subsequent regression analyses. Differential SCR (i.e., CS+ minus CS− responses averaged across the 7 trials of each) was calculated as a measure of fear learning, as well as average CS+ and CS− responses versus the implicit baseline.

Functional MRI procedures

fMRI was performed with a Trio 3.0 Tesla whole-body, MRI system (Siemens Medical Systems, Iselin, New Jersey) equipped for echo planar imaging (EPI) with a 32-channel head coil. Subjects were instructed to lie as still as possible and head movement was restricted with foam cushions. After an automated scout image was obtained and automated shimming procedures were performed, a high-resolution structural scan was collected to facilitate spatial normalization and to position the subsequent scans. fMRI images, sensitive to BOLD contrast, were acquired during fear conditioning with a descending gradient echo T2*-weighted sequence (TR= 2560 ms, TE= 30ms, Flip angle = 90°), collected in 48 coronal oblique slices tilted 38° down from the anterior-posterior commissure line. The voxel size was 3×3×2.5 mm with a 0.5 mm slice gap. The field of view was 144 mm (whole brain down to medulla).

Data preprocessing, analysis and statistical inferences

SPM8 (www.fil.ion.ucl.ac.uk) was used to process all PET and MRI data. For the PET analysis, each subject's static FDG image was co-registered to individual high-resolution structural MRI images. Structural images were segmented, bias correct and spatially normalized (Ashburner and Friston, 2005) into MNI space and normalization parameters were applied to the PET images, which were then smoothed (8 mm full-width at half-maximum, FWHM) and finally global mean normalized to 50.

Functional images were realigned, corrected for slice timing, co-registered with the structural image, normalized into MNI space using parameters obtained from the structural normalization process, and finally smoothed with an 8 mm FWHM Gaussian kernel. Maximal movement in any direction in all data was 3.58 mm or 3.4º. After preprocessing, each subject's functional time series was modeled using a general linear model with regressors signifying the condition onsets and durations. The experimental conditions were: the context, the first 7 CS+, the second 8 CS+ (not reported) the first 7 CS−, the second 8 CS− (not reported) and the US. The responses to the very first CS+ and CS− cue, i.e prior to any conditioning, and movement parameters from the realignment step for x,y,z, and roll, pitch and yaw motion were also included in the model. Signal drift and biorhythms were modeled using high-pass temporal filtering (128s) and an autoregressive AR-1 model. Activated voxels in each experimental condition were identified using a statistical model containing boxcar functions representing the contrasts of interest, convolved with the SPM8 canonical hemodynamic response function.

Statistical thresholds

For all neuroimaging analyses, we used a statistical threshold of $p<0.05$ family wise error corrected for multiple comparisons. Within our *a priori* fear network, we used a more liberal threshold of $p<0.005$ uncorrected for multiple comparisons. The *a priori* network was defined using the AAL masks in the WFU pickatlas (Lancaster et al., 2000; Maldjian et al., 2003) for the left and right amygdala, the left and right insula, the left and right ACC and middle cingulate, and the midbrain. The vmPFC was defined as a 10 mm radius sphere centered at $MNI_{x,y,z}$ = 4, 36, −13 (coordinates obtained from Milad et al., 2005).

Autonomic correlates of resting state metabolism

Average differential SCR (CS+ versus CS−) was used as a linear regressor on the resting state metabolism data in order to test for regions where individual metabolism measures predicted subsequent fear learning. In addition, SCR responses to the CS+ alone and the CS − alone were also used as regressors.

Fear induced BOLD activations and autonomic correlates

First, contrast images signifying the difference in BOLD reactivity to the first 7 CS+ versus the first 7 CS− trials were obtained within each subject (first level model) and then modeled at the second level using a random effects t-test. Third, differential SCR was entered into a linear regression model for the above BOLD contrast. As a core feature of maladaptive anxiety may be heightened responses to a CS− (Lissek et al., 2005), we also analyzed skin conductance and functional responses to the CS+ and the CS− separately contrasted against the implicit inter-trial baseline.

Resting brain metabolism correlates of functional activation during fear conditioning

A priori, we were interested in the influence of the midbrain, amygdala, dACC, anterior insula and vmPFC on acquisition of conditioned fear. Performing voxelwise (metabolism) × voxelwise (BOLD) analyses creates massive multiple comparisons. Instead, we created five predefined anatomical regions of interest (ROIs, viz., midbrain, amygdala, dACC, insula, vmPFC) and extracted each subjects average regional cerebral metabolic rate for glucose (rCMRglu) in those regions. The midbrain was defined as a 5 mm sphere centered at $MNI_{x,y,z}$ = 0, 30, −12, corresponding to the periaqueductal gray region. The left and right amygdala (combined) were defined by the AAL atlas (Tzourio-Mazoyer et al., 2002). The dACC ROI was a 5 mm sphere at $MNI_{x,y,z}$ = 2, 22, 28 (from Milad et al., 2007a). The combined left and right anterior insula was two 5 mm spheres at $MNI_{x,y,z}$ = ±34, 20, −4 (coordinates from anatomy), and the vmPFC was a was a 5 mm sphere centered at $MNI_{x,y,z}$ = 4, 36, −13 (coordinates obtained from Milad et al., 2005).

Average rCMRglu from the five *a priori* ROIs were entered separately into voxelwise linear regression models to investigate their respective influences on BOLD reactivity in the differential fear conditioning fMRI contrast.

Results

Subjects selected shock levels at an average of 2.1mA (range 1.1 – 4.0 mA). Due to technical difficulties, adequate skin conductance measures were only obtained in 17 of the 20 subjects. Fear conditioning led to rapid acquisition of conditioned responses; the mean (± standard deviation) differential SCR was 0.46±0.27 $\mu S^{-½}$, p<0.00l. The unconditioned stimulus also led to an unconditioned response, with a mean SCR to the US of 1.38±0.24 $\mu S^{-½}$, p<0.00l. See supplemental figure S1 for trial-by-trial responses.

fMRI data of sufficient quality was obtained from all 20 subjects.

Fear conditioning, whole brain analysis

Fear conditioning induced significant activations in the midbrain, amygdala, putamen, anterior and middle cingulate insula, cerebellum and frontal cortices, see Table 1 and Figure 1 for details. The CS+ versus the inter-trial baseline activated similar regions and also the visual cortex. The CS− versus baseline activated predominantly the visual cortex, see supplemental figure S2 and table S1.

BOLD correlations to SCR, whole brain

In the whole brain analysis, positive correlations between differential SCR and differential BOLD signal were observed in the bilateral middle frontal gyrus and in the left hippocampus region, see Figure 2 and Table 2 for details. No regions displayed negative correlations between SCR and BOLD response. See supplementary table S2 for correlations between CS+ and CS− SCR responses and BOLD responses to CS+, and CS−, vs. the inter-trial baseline.

BOLD correlations to SCR, a priori fear regions

Within the *a priori* fear network, positive correlations between differential SCR responses and differential BOLD signal (CS+ versus CS−) were observed in the right anterior insula and in the midbrain, see Figure 2.

Question one: Can regional resting metabolism predict the magnitude of autonomic fear responses?

There were no correlations between autonomic responses and whole brain resting metabolism that survived corrections for multiple comparisons.

Within the *a priori* fear network, right resting dACC metabolism positively predicted differential SCR during fear conditioning. Midbrain and cerebellar resting metabolism were negative predictors. See figure 3 and table 3 for details. Of note, dACC metabolism also predicted CS+ alone SCR responses, and genual ACC predicted CS− alone SCR responses, see supplemental figure S3 and table S3 for details.

Question two: Can resting metabolism predict the magnitude of BOLD activations during fear acquisition?

In the whole brain analysis, dACC metabolism correlated with occipital and parietal BOLD activations, see table 4b for details

Within the *a priori* fear network, several significant correlations were apparent: Midbrain metabolism negatively predicted midbrain BOLD signal (Figure 4a and Table 4a). dACC metabolism positively predicted midbrain BOLD signal (Figure 4b and Table 4b). Anterior insula metabolism negatively predicted subgenual ACC and middle right insula BOLD signal (Figure 4c and Table 4c). Amygdala metabolism negatively predicted BOLD signal in the left anterior insula (Figure 4d and table 4d). No significant predictions of BOLD signal were observed for the vmPFC.. Relations between metabolism and BOLD responses to the CS+ (versus implicit baseline) and responses to the CS− (versus implicit baseline) are reported in supplemental table S4.

Discussion

The fear conditioning paradigm led to strong conditioned physiological and neuronal responses, consistent with previous reports (reviewed in Sehlmeyer et al., 2009). When we explored links between resting brain metabolism and these responses, several findings emerged.

Question one: Can resting brain metabolism predict autonomic responses during fear acquisition?

In line with our hypothesis, we found that resting metabolism in the dACC positively predicted the acquisition of differential skin conductance responses to the CS+ versus CS−,

which is an autonomic measure of conditioned fear. The correlation between dACC metabolism and SCR was also present to the CS+ alone SCR, suggesting it was primarily driven by the emotional content of the CS+ and not a function of autonomic reactivity in general. This is perhaps the most readily interpretable and important finding of the present study. It is consistent with the finding that structural thickness of the dACC positively correlates with the magnitude of conditioned responses (Milad et al., 2007a), studies on control of autonomic arousal during volitional behaviors (Critchley, 2005), and with the finding that direct electrical stimulation of this region results in skin conductance responses (Gentil et al., 2009). Our finding is also consistent with converging evidence that the dACC is involved in negative affect (Shackman et al., 2011). As noted above, clinical studies have shown that both elevated resting metabolism and elevated functional reactivity in dACC constitutes a familial risk factor for the development of PTSD (Shin et al., 2011; Shin et al., 2009). The present results offer an insight into how this risk factor may operate. Specifically, fear conditioning is a frequently invoked pathogenic mechanism in PTSD (Rauch et al., 2006). Anything that increases fear learning, such as elevated dACC metabolism, would logically increase the likelihood of PTSD‘s developing following the requisite traumatic event. We also observed a positive correlation between resting dACC metabolism and midbrain BOLD reactivity (figure 4c).

High differential skin conductance responses were associated with high midbrain BOLD reactivity (Figure 2) and with low midbrain resting metabolism. Furthermore, low midbrain metabolism was associated with high midbrain BOLD reactivity. Though apparently inconsistent with the directionality of our findings, elevated midbrain metabolism has been observed in panic disorder patients (Sakai et al., 2005) and in anxious rhesus monkeys (Fox et al., 2008). The brain region we observed to be correlated with conditioned responses appears in close proximity to the PAG. However, midbrain regions contain several subnuclei involved in opposing behavior such as fight-flight and hypertension (lateral PAG) or quiescence and hypotension (ventrolateral PAG) (Behbehani, 1995) and the specific role of the midbrain regions in our data is not possible to discern at the current spatial resolution (Limbrick-Oldfield et al., 2011). For example, lesions in the midbrain ascending noradrenergic bundle abolishes skin conductance responses via hypothalamic and amygdala effects (Yamamoto et al., 1990).

Previous human neuroimaging studies that indicate orbitofrontal and medial prefrontal cortex and amygdala influences on lateral hypothalamus and brainstem mechanisms controlling skin conductance (Critchley et al., 2000; Nagai et al., 2004; Williams et al., 2001). Particularly, the human amygdala activity is closely related to the expression of conditional SCRs (Cheng et al., 2007). We did not find evidence for a correlation between resting metabolism in the amygdala and evoked SCR, nor did we observe a correlation between differential SCR and differential BOLD reactivity in the amygdala or in the medial prefrontal cortex. One possible explanation for this discrepancy is that the above studies used the SCR as a temporally continuous variable, whereas we investigated the average SCR evoked across 7 trials each lasting 6 seconds, and related those to the corresponding evoked BOLD signal. Amygdala activation corresponds to the early SCR response evoked by presentation of a conditioned cue, but not to SCR’s evoked towards the end of the cue presentation, just before the delivery of the US (Cheng et al., 2007). A higher temporal resolution may thus be necessary to identify the amygdala’s (and possibly the dACC and hypothalamus) role in generating SCRs.

Question two: Can resting brain metabolism predict brain activation during fear acquisition?

In addition to the negative correlation between resting midbrain metabolism and midbrain BOLD signal during conditioning discussed above, there was a negative correlation between

insula metabolism and insula BOLD reactivity (figure 4c). Moreover, higher insula BOLD reactivity related to greater SCRs (figure 2), consistent with previous studies (see Critchley, 2005 for a review). In addition, we found that high resting amygdala metabolism was predictive of low insula BOLD reactivity. Unlike the amygdala and the dACC, insula BOLD reactivity has been found to increase when there is uncertainty with respect to the contingency between cue and shock (Dunsmoor et al., 2007; Sarinopoulos et al., 2010). The anterior insula has been theorized to function as a re-representation region where anticipated interoceptive emotions can be simulated in advance (Craig, 2009). In light of this view, the present observation that both insula and amygdala metabolism negatively predicted insula BOLD activation may suggest that individuals with high amygdala metabolism are less able to determine the degree of uncertainty of impending threats, and thus engage in less anticipatory insula activation, but this speculation is in need of further testing.

We did not observe any correlation between amygdala metabolism and amygdala reactivity, nor between amygdala metabolism or BOLD signal and the magnitude of differential skin conductance responses, as has been reported in other studies (Furmark et al., 1997; Indovina et al., 2011). We did however observe a positive correlation between amygdala BOLD reactivity to the CS+ and the CS+ induced SCR (supplemental table S3). This would suggest that the amygdala is involved in fear learning, but not in the safety learning associated with a non-reinforced CS−.

Heightened responses to a CS−, a “safety signal deficit”, have been argued to be a core feature of maladaptive anxiety (Lissek et al., 2005). We observed a positive correlation between genual ACC metabolism and CS− SCR responses (supplemental Table S3) and a negative correlation between CS− BOLD reactivity in the subgenual ACC/ventromedial prefrontal corex. The latter finding is consistent with a safety signaling role of the vmPFC, as has been observed in numerous studies (reviewed in Milad and Rauch, 2007).

Limitations

Autonomic and fMRI measurements were obtained simultaneously during conditioning, but resting metabolic measures were obtained approximately 2 days prior to conditioning. We assumed that resting metabolism would be stable over time, and good test-retest reliability over 6 months has been reported for thalamus, hippocampus and left (but not right) amygdala (Schaefer et al., 2000). Thus, future studies could benefit from more closely spaced or simultaneous PET and fMRI assessments (Judenhofer et al., 2008). Unfortunately, we did not collect contingency learning ratings for the participants, such ratings may have allowed for further differentiation and detailing of neuronal responses (Tabbert et al., 2010). Another limitation arises from potential noise sources in the PET and fMRI data. FDG PET is relatively insensitive to movement compared to fMRI BOLD; we attempted to remove PET movement artifacts in the procedure and fMRI movements in the procedure and data analysis. Moreover, both PET and fMRI have limited spatial resolution and thus likely obscure finer anatomical details, especially in small structures such as the periaqueductal gray and the amygdala that contain substructures that may exert opposing influences on behavior. Using imaging techniques with greater spatial resolution could help address this problem. The correlation coefficients reported in the tables are likely to be inflated due to the low sample size and the voxel vise regression approach (Vul et al., 2009; Yarkoni, 2009). They should thus be interpreted with caution. Another possibility, which we did not explore here, would be to use functional connectivity MRI measure to predict subsequent functional reactivity (Liu et al., 2011; Ploner et al., 2010) and behavior (Lanius et al., 2010; Shannon et al., 2011).

Conclusions

With regards to our first question, viz., can we predict fear learning, both resting dACC and midbrain metabolism successfully predicted a subsequent autonomic measure of fear conditioning. The relationship between resting metabolism and subsequent brain reactivity to conditioned cues appears to be more ambiguous and complex. Within two regions, the midbrain and the anterior insula, there was a negative relationship between the resting metabolism and subsequent functional reactivity in the same region. For the amygdala and the dACC, this was not the case. Instead, resting metabolism in the amygdala and dACC predicted insula and midbrain reactivity, respectively. A general conclusion is that individual differences in the baseline metabolic demand of a region may influence other regions' functional reactivity, indicating new relationships that constitute a more complete picture of intrinsic brain activity and stimulus-induced activation changes that require further clarification. Future studies will likely benefit from obtaining resting measures, either by FDG PET as we did, or by resting state connectivity or arterial spin labeling methods.

Supplementary Material

Refer to Web version on PubMed Central for supplementary material.

Acknowledgments

This work was supported by Institute of Mental Health grant 1R01MH081975-01 (MGH subcontract) to M.R.M.

References

Ashburner J, Friston KJ. Unified segmentation. NeuroImage. 2005; 26:839–851. [PubMed: 15955494]

Behbehani MM. Functional characteristics of the midbrain periaqueductal gray. Progress in neurobiology. 1995; 46:575–605. [PubMed: 8545545]

Cheng DT, Richards J, Helmstetter FJ. Activity in the human amygdala corresponds to early, rather than late period autonomic responses to a signal for shock. Learning & memory. 2007; 14:485–490. [PubMed: 17626906]

Craig AD. How do you feel--now? The anterior insula and human awareness. Nat Rev Neurosci. 2009; 10:59–70. [PubMed: 19096369]

Critchley HD. Neural mechanisms of autonomic, affective, and cognitive integration. J Comp Neurol. 2005; 493:154–166. [PubMed: 16254997]

Critchley HD, Elliott R, Mathias CJ, Dolan RJ. Neural activity relating to generation and representation of galvanic skin conductance responses: a functional magnetic resonance imaging study. The Journal of neuroscience: the official journal of the Society for Neuroscience. 2000; 20:3033–3040. [PubMed: 10751455]

Dunsmoor JE, Bandettini PA, Knight DC. Impact of continuous versus intermittent CS−UCS pairing on human brain activation during Pavlovian fear conditioning. Behavioral neuroscience. 2007; 121:635–642. [PubMed: 17663589]

Etkin A, Wager TD. Functional Neuroimaging of Anxiety: A Meta-Analysis of Emotional Processing in PTSD, Social Anxiety Disorder, and Specific Phobia. Am J Psychiatry. 2007; 164:1476–1488. [PubMed: 17898336]

Fox AS, Shelton SE, Oakes TR, Davidson RJ, Kalin NH. Trait-like brain activity during adolescence predicts anxious temperament in primates. PloS one. 2008; 3:e2570. [PubMed: 18596957]

Furmark T, Fischer H, Wik G, Larsson M, Fredrikson M. The amygdala and individual differences in human fear conditioning. Neuroreport. 1997; 8:3957–3960. [PubMed: 9462473]

Fusar-Poli P, Placentino A, Carletti F, Landi P, Allen P, Surguladze S, Benedetti F, Abbamonte M, Gasparotti R, Barale F, Perez J, McGuire P, Politi P. Functional atlas of emotional faces

processing: a voxel-based meta-analysis of 105 functional magnetic resonance imaging studies. J Psychiatry Neurosci. 2009; 34:418–432. [PubMed: 19949718]

Gentil AF, Eskandar EN, Marci CD, Evans KC, Dougherty DD. Physiological responses to brain stimulation during limbic surgery: further evidence of anterior cingulate modulation of autonomic arousal. Biol Psychiatry. 2009; 66:695–701. [PubMed: 19545859]

Graham BM, Milad MR. The Study of Fear Extinction: Implications for Anxiety Disorders. Am J Psychiatry. 2011

Indovina I, Robbins TW, Nunez-Elizalde AO, Dunn BD, Bishop SJ. Fear-conditioning mechanisms associated with trait vulnerability to anxiety in humans. Neuron. 2011; 69:563–571. [PubMed: 21315265]

Johansen JP, Tarpley JW, LeDoux JE, Blair HT. Neural substrates for expectation-modulated fear learning in the amygdala and periaqueductal gray. Nature neuroscience. 2010; 13:979–986.

Judenhofer MS, Wehrl HF, Newport DF, Catana C, Siegel SB, Becker M, Thielscher A, Kneilling M, Lichy MP, Eichner M, Klingel K, Reischl G, Widmaier S, Rocken M, Nutt RE, Machulla HJ, Uludag K, Cherry SR, Claussen CD, Pichler BJ. Simultaneous PET-MRI: a new approach for functional and morphological imaging. Nature medicine. 2008; 14:459–465.

Kalisch R, Korenfeld E, Stephan KE, Weiskopf N, Seymour B, Dolan RJ. Context-dependent human extinction memory is mediated by a ventromedial prefrontal and hippocampal network. J Neurosci. 2006; 26:9503–9511. [PubMed: 16971534]

Lancaster JL, Woldorff MG, Parsons LM, Liotti M, Freitas CS, Rainey L, Kochunov PV, Nickerson D, Mikiten SA, Fox PT. Automated Talairach atlas labels for functional brain mapping. Hum Brain Mapp. 2000; 10:120–131. [PubMed: 10912591]

Lanius RA, Bluhm RL, Coupland NJ, Hegadoren KM, Rowe B, Theberge J, Neufeld RW, Williamson PC, Brimson M. Default mode network connectivity as a predictor of post-traumatic stress disorder symptom severity in acutely traumatized subjects. Acta Psychiatr Scand. 2010; 121:33–40. [PubMed: 19426163]

Limbrick-Oldfield EH, Brooks JC, Wise RJ, Padormo F, Hajnal JV, Beckmann CF, Ungless MA. Identification and characterisation of midbrain nuclei using optimised functional magnetic resonance imaging. NeuroImage. 2011

Linnman C, Rougemont-Bucking A, Beucke JC, Zeffiro TA, Milad MR. Unconditioned responses and functional fear networks in human classical conditioning. Behavioural brain research. 2011; 221:237–245. [PubMed: 21377494]

Linnman C, Zeidan MA, Furtak SC, Pitman RK, Quirk GJ, Milad MR. Resting amygdala and medial prefrontal metabolism predicts functional activation of the fear extinction circuit. Am J Psychiatry. in press.

Lissek S, Powers AS, McClure EB, Phelps EA, Woldehawariat G, Grillon C, Pine DS. Classical fear conditioning in the anxiety disorders: a meta-analysis. Behaviour Research and Therapy. 2005; 43:1391–1424. [PubMed: 15885654]

Liu X, Zhu XH, Chen W. Baseline BOLD correlation predicts individuals' stimulus-evoked BOLD responses. NeuroImage. 2011; 54:2278–2286. [PubMed: 20934521]

Logothetis NK. The neural basis of the blood-oxygen-level-dependent functional magnetic resonance imaging signal. Philosophical transactions of the Royal Society of London. 2002; 357:1003–1037. [PubMed: 12217171]

Maldjian JA, Laurienti PJ, Burdette JB, Kraft RA. An Automated Method for Neuroanatomic and Cytoarchitectonic Atlas-based Interrogation of fMRI Data Sets. NeuroImage. 2003; 19:1233–1239. [PubMed: 12880848]

Milad MR, Pitman RK, Ellis CB, Gold AL, Shin LM, Lasko NB, Zeidan MA, Handwerger K, Orr SP, Rauch SL. Neurobiological basis of failure to recall extinction memory in posttraumatic stress disorder. Biol Psychiatry. 2009; 66:1075–1082. [PubMed: 19748076]

Milad MR, Quinn BT, Pitman RK, Orr SP, Fischl B, Rauch SL. Thickness of ventromedial prefrontal cortex in humans is correlated with extinction memory. Proc Natl Acad Sci U S A. 2005; 102:10706–10711. [PubMed: 16024728]

Milad MR, Quirk GJ, Pitman RK, Orr SP, Fischl B, Rauch SL. A role for the human dorsal anterior cingulate cortex in fear expression. Biol Psychiatry. 2007a; 62:1191–1194. [PubMed: 17707349]

Milad MR, Rauch SL. The role of the orbitofrontal cortex in anxiety disorders. Ann N Y Acad Sci. 2007; 1121:546–561. [PubMed: 17698998]

Milad MR, Wright CI, Orr SP, Pitman RK, Quirk GJ, Rauch SL. Recall of fear extinction in humans activates the ventromedial prefrontal cortex and hippocampus in concert. Biol Psychiatry. 2007b; 62:446–454. [PubMed: 17217927]

Nagai Y, Critchley HD, Featherstone E, Trimble MR, Dolan RJ. Activity in ventromedial prefrontal cortex covaries with sympathetic skin conductance level: a physiological account of a “default mode” of brain function. NeuroImage. 2004; 22:243–251. [PubMed: 15110014]

Napadow V, Dhond R, Conti G, Makris N, Brown EN, Barbieri R. Brain correlates of autonomic modulation: combining heart rate variability with fMRI. NeuroImage. 2008; 42:169–177. [PubMed: 18524629]

Nili U, Goldberg H, Weizman A, Dudai Y. Fear thou not: activity of frontal and temporal circuits in moments of real-life courage. Neuron. 2010; 66:949–962. [PubMed: 20620879]

Ogawa S, Lee TM, Nayak AS, Glynn P. Oxygenation-sensitive contrast in magnetic resonance image of rodent brain at high magnetic fields. Magnetic resonance in medicine: official journal of the Society of Magnetic Resonance in Medicine/Society of Magnetic Resonance in Medicine. 1990; 14:68–78. [PubMed: 2161986]

Phelps EA, Delgado MR, Nearing KI, LeDoux JE. Extinction learning in humans: role of the amygdala and vmPFC. Neuron. 2004; 43:897–905. [PubMed: 15363399]

Phelps EA, LeDoux JE. Contributions of the amygdala to emotion processing: from animal models to human behavior. Neuron. 2005; 48:175–187. [PubMed: 16242399]

Ploner M, Lee MC, Wiech K, Bingel U, Tracey I. Prestimulus functional connectivity determines pain perception in humans. Proc Natl Acad Sci U S A. 2010; 107:355–360. [PubMed: 19948949]

Raichle ME, Mintun MA. Brain work and brain imaging. Annu Rev Neurosci. 2006; 29:449–476. [PubMed: 16776593]

Rauch SL, Shin LM, Phelps EA. Neurocircuitry models of posttraumatic stress disorder and extinction: human neuroimaging research--past, present, and future. Biol Psychiatry. 2006; 60:376–382. [PubMed: 16919525]

Sakai Y, Kumano H, Nishikawa M, Sakano Y, Kaiya H, Imabayashi E, Ohnishi T, Matsuda H, Yasuda A, Sato A, Diksic M, Kuboki T. Cerebral glucose metabolism associated with a fear network in panic disorder. Neuroreport. 2005; 16:927–931. [PubMed: 15931063]

Sarinopoulos I, Grupe DW, Mackiewicz KL, Herrington JD, Lor M, Steege EE, Nitschke JB. Uncertainty during anticipation modulates neural responses to aversion in human insula and amygdala. Cereb Cortex. 2010; 20:929–940. [PubMed: 19679543]

Schaefer SM, Abercrombie HC, Lindgren KA, Larson CL, Ward RT, Oakes TR, Holden JE, Perlman SB, Turski PA, Davidson RJ. Six-month test-retest reliability of MRI-defined PET measures of regional cerebral glucose metabolic rate in selected subcortical structures. Hum Brain Mapp. 2000; 10:1–9. [PubMed: 10843513]

Sehlmeyer C, Schoning S, Zwitserlood P, Pfleiderer B, Kircher T, Arolt V, Konrad C. Human fear conditioning and extinction in neuroimaging: a systematic review. PloS one. 2009; 4:e5865. [PubMed: 19517024]

Shackman AJ, Salomons TV, Slagter HA, Fox AS, Winter JJ, Davidson RJ. The integration of negative affect, pain and cognitive control in the cingulate cortex. Nat Rev Neurosci. 2011; 12:154–167. [PubMed: 21331082]

Shannon BJ, Raichle ME, Snyder AZ, Fair DA, Mills KL, Zhang D, Bache K, Calhoun VD, Nigg JT, Nagel BJ, Stevens AA, Kiehl KA. Premotor functional connectivity predicts impulsivity in juvenile offenders. Proc Natl Acad Sci U S A. 2011; 108:11241–11245. [PubMed: 21709236]

Shin LM, Bush G, Milad MR, Lasko NB, Brohawn KH, Hughes KC, Macklin ML, Gold AL, Karpf RD, Orr SP, Rauch SL, Pitman RK. Exaggerated Activation of Dorsal Anterior Cingulate Cortex During Cognitive Interference: A Monozygotic Twin Study of Posttraumatic Stress Disorder. Am J Psychiatry. 2011

Shin LM, Lasko NB, Macklin ML, Karpf RD, Milad MR, Orr SP, Goetz JM, Fischman AJ, Rauch SL, Pitman RK. Resting metabolic activity in the cingulate cortex and vulnerability to posttraumatic stress disorder. Archives of general psychiatry. 2009; 66:1099–1107. [PubMed: 19805700]

Shin LM, Liberzon I. The neurocircuitry of fear, stress, and anxiety disorders. Neuropsychopharmacology. 2010; 35:169–191. [PubMed: 19625997]

Sokoloff L. Relation between physiological function and energy metabolism in the central nervous system. Journal of neurochemistry. 1977; 29:13–26. [PubMed: 407330]

Tabbert K, Merz CJ, Klucken T, Schweckendiek J, Vaitl D, Wolf OT, Stark R. Influence of contingency awareness on neural, electrodermal and evaluative responses during fear conditioning. Social cognitive and affective neuroscience. 2010

Tzourio-Mazoyer N, Landeau B, Papathanassiou D, Crivello F, Etard O, Delcroix N, Mazoyer B, Joliot M. Automated anatomical labeling of activations in SPM using a macroscopic anatomical parcellation of the MNI MRI single-subject brain. Neuroimage. 2002; 15:273–289. [PubMed: 11771995]

Vul E, Harris C, Winkielman P, Pashler H. Puzzlingly high correlations in fMRI studies of emotion, personality, and social cognition. Perspectives on Psychological Science. 2009; 4:274–290.

Williams LM, Phillips ML, Brammer MJ, Skerrett D, Lagopoulos J, Rennie C, Bahramali H, Olivieri G, David AS, Peduto A, Gordon E. Arousal dissociates amygdala and hippocampal fear responses: evidence from simultaneous fMRI and skin conductance recording. NeuroImage. 2001; 14:1070–1079. [PubMed: 11697938]

Yarkoni T. Big Correlations in Little studies. Perspectives on Psychological Science. 2009; 4:295–298.

Highlights

Regional resting glucose metabolism measured via positron emission tomography, skin conductance and and functional MRI responses during fear conditioning, were obtained from 20 healthy individuals.

Resting anterior mid-cingulate metabolism was positively, and resting midbrain metabolism negatively, correlated with the acquisition of autonomic conditioned fear responses, as measured via skin conductance.

Anterior insula and midbrain resting metabolism negatively correlated with their subsequent BOLD reactivity to fear learning, while resting dACC metabolism predicted midbrain BOLD reactivity. The results indicate a complex relationship between resting metabolism and individual variation in fear learning.

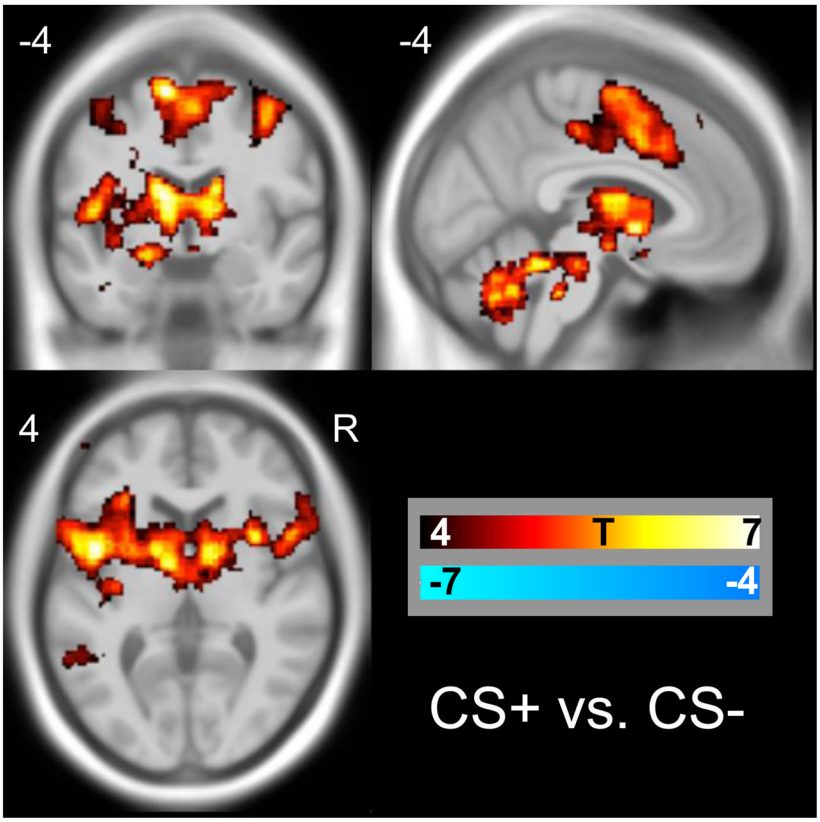

Figure 1. Regions activated by fear conditioning

BOLD responses (CS+ minus CS−) in the whole brain analysis overlaid on an MNI template. In all figures, activations and positive correlations are shown in warm colours, deactivations and negative correlations are shown in cool colours, as indicated by the colour bar.

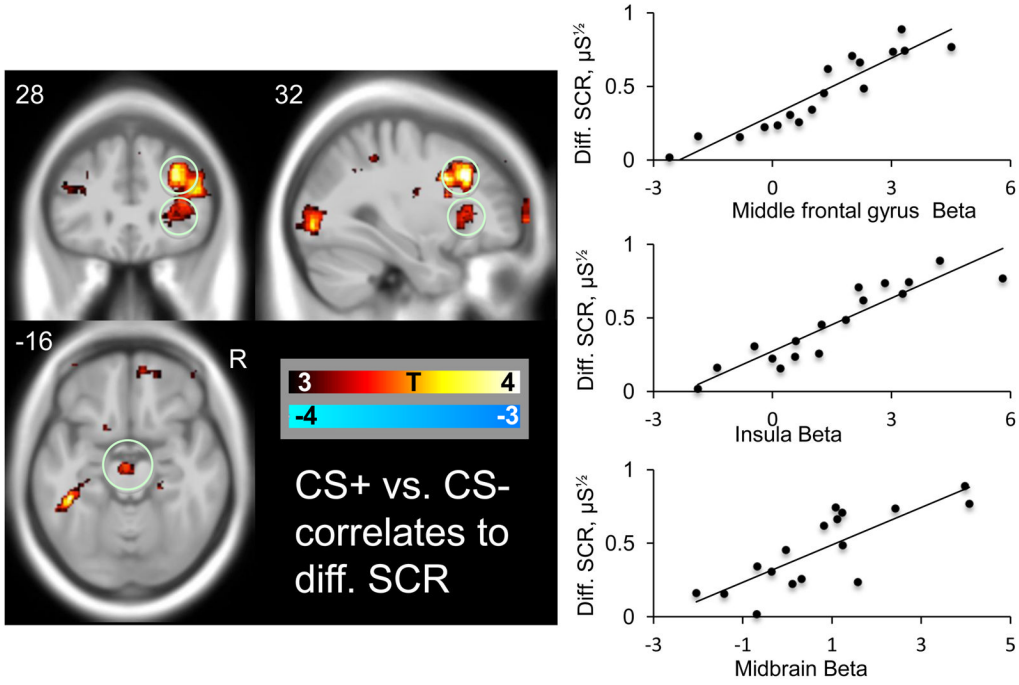

Figure 2. OLD correlates ofautonomic fear responses

Correlations between conditioned BOLD and conditioned skin conductance responses in the whole brain analysis overlaid on an MNI template. The scatter plot indicates the correlation between BOLD beta estimates (CS+ vs. CS+) in the circled middle frontal gyrus, and in our *a priori* fear network regions: the insula and midbrain cluster and differential skin conductance responses (CS+ minus CS−).

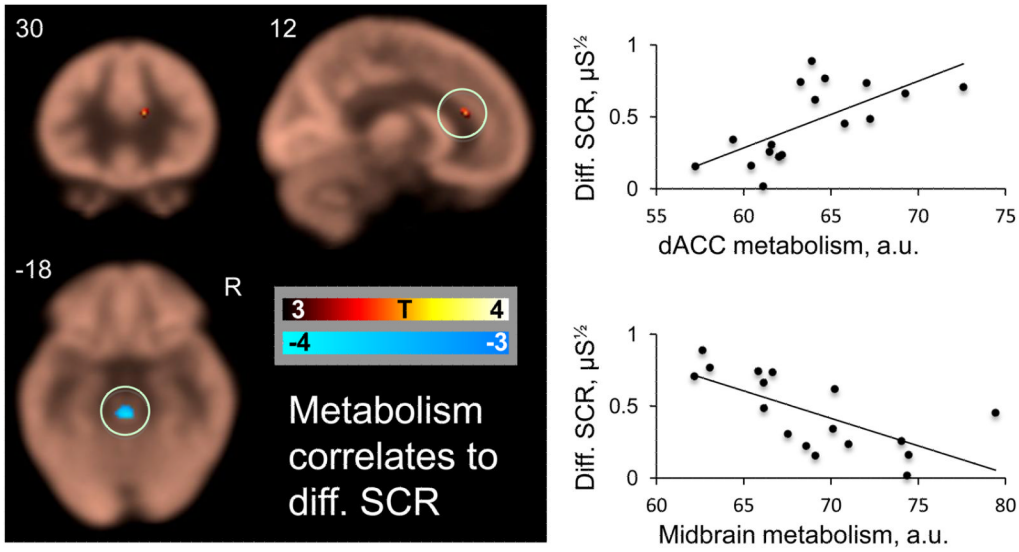

Figure 3. Resting brain metabolism predicts autonomic fear responses

Correlations between resting cerebral metabolic rate for glucose and differential conditioned skin conductance responses. The average FDG map is displayed in beige, overlaid with the metabolism-SCR correlation map masked with our *a priori* regions of interest The scatter plots indicate the correlation between the circled dACC and midbrain clusters and differential SCR.

Figure 4a

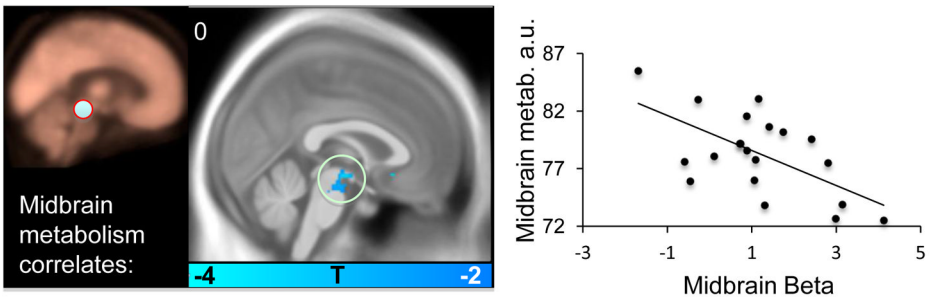

Figure 4b

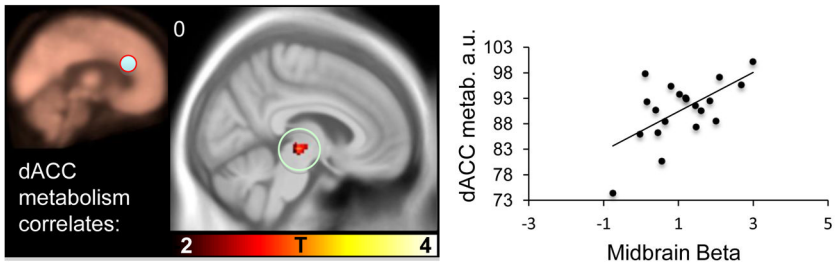

Figure 4c

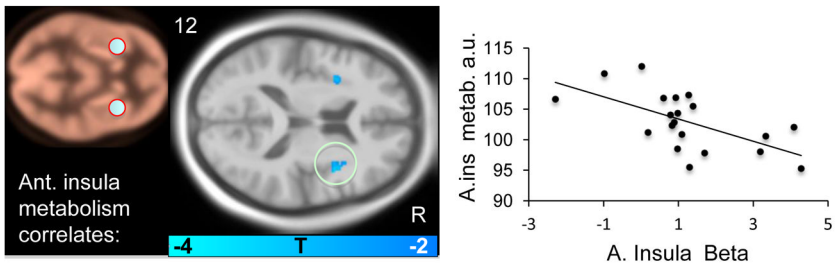

Figure 4d

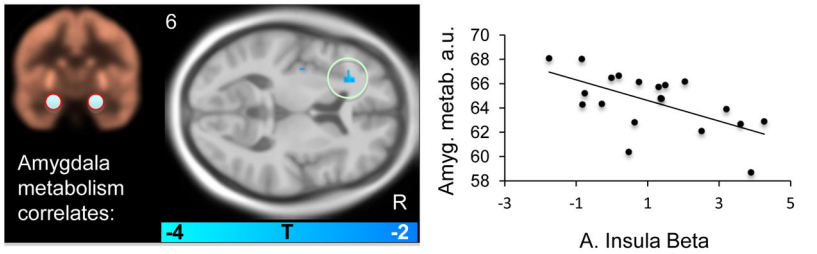

Figure 4a–d. Resting brain metabolism predicts BOLD signal responses

Correlations between resting metabolism and differential BOLD (CS+ vs. CS−) are displayed on an MNI template masked with our *a priori* regions of interest. The metabolism regions of interest is indicated on the beige metabolism map and the scatter plot illustrates the observed correlations for a) midbrain, b) dACC, c) anterior insula and d) amygdala metabolism and BOLD beta values.

Biol Psychol. Author manuscript; available in PMC 2013 February 1.

Table 1

BOLD responses to fear conditioning (CS+ minus CS−)

cluster p(FWE-cor)	cluster size (voxels)	peak equivZ	peak p(unc)	MNI x,y,z	Peak region
Whole brain					
0	70495	6.85	0.000	−32 −10 50	Left Middle Frontal Gyrus
		6.65	0.000	−2 2 −4	Left Anterior Cingulate
		6.58	0.000	10 4 56	Right Medial Frontal Gyrus
		4.7	0.000	38 −20 −6	Right Claustrum
0.029	237	4.51	0.000	34 −26 0	Right Putamen
		3.54	0.000	32 −16 −16	Right Hippocampus
0.001	498	4.47	0.000	12 72 −6	Right Superior Frontal Gyrus
		4.06	0.000	0 68 2	Left Medial Frontal Gyrus
		3.94	0.000	−6 72 10	Left Medial Frontal Gyrus
0.003	378	3.91	0.000	36 66 2	Right Superior Frontal Gyrus
		3.75	0.000	36 48 20	Right Middle Frontal Gyrus
		3.71	0.000	36 60 10	Right Middle Frontal Gyrus
Fear network ROIs					
Amygdala					
	60	4.37	0.000	20 0 −12	Right Parahippocampal Gyrus
		2.69	0.004	32 −2 −12	Right Amygdala
	171	4.36	0.000	−12 −2 −16	Left Parahippocampal Gyrus
		3.18	0.001	−30 −2 −28	Left Amygdala
		3.17	0.001	−22 2 −24	Left Amygdala
Anterior and middle cingulate					
	1281	5.03	0.000	−10 34 18	Left Anterior Cingulate
		4.87	0.000	−4 28 16	Left Anterior Cingulate
		4.51	0.000	6 28 18	Right Anterior Cingulate
	7	3.71	0.000	2 20 −8	Right Anterior Cingulate
Insula					
	1693	6.29	0.000	−34 −2 8	Left Claustrum
		5.8	0.000	−32 −20 6	Left Claustrum
		5.7	0.000	−28 18 −4	Left Insula

cluster p(FWE-cor)	cluster size (voxels)	peak equivZ	peak p(unc)	MNI x,y,z	Peak region
	1193	5.47	0.000	32 14 6	Right Claustrum
		4.34	0.000	26 18 −18	Right Inferior Frontal Gyrus/insula
		4.29	0.000	32 18 −10	Right anterior insula
	43	3.43	0.000	38 −28 22	Right Posterior Insula
		3.18	0.001	32 −20 22	Right Posterior Insula
Midbrain					
	1890	5.96	0.000	6 −4 −2	Right Hypothalamus*
		5.94	0.000	−8 −14 −12	Left Substania Nigra*
		5.64	0.000	8 −18 −4	Right Red Nucleus*
vmPFC					
	No significant clusters				

*approximate locations. No deactivated regions were observed in the whole brain or ROI analyses

Table 2

Significant correlations between differential skin conductance responses and differential BOLD responses

cluster p(FWE-cor)	cluster size (voxels)	Z	r^2	peak p(unc)	MNI x,y,z	Peak region
Whole brain						
Positive correlations						
0	1302	5.47	0.84	0.000	38 10 30	Right Middle Frontal Gyrus
		4.69		0.000	34 24 32	Right Middle Frontal Gyrus
		4.31		0.000	60 18 28	Right Inferior Frontal Gyrus
0.029	217	4.58	0.65	0.000	−44 −40 −14	Left Fusiform Gyrus
		3.74		0.000	−34 −30 −10	Left Hippocampus
		3.49		0.000	−54 −40 −6	Left Middle Temporal Gyrus
0.029	216	4.42	0.64	0.000	26 −84 −2	Right Middle Occipital Gyrus
0.001	431	4.15	0.69	0.000	−44 18 30	Left Middle Frontal Gyrus
		4.06		0.000	−36 14 44	Left Precentral Gyrus
		3.89		0.000	−52 18 38	Left Middle Frontal Gyrus
Fear network ROIs						
Positive correlations						
	64	3.83	0.60	0.000	−2 −14 −16	Midbrain
	34	3.59	0.50	0.000	34 −12 16	Right Anterior/Middle Insula
	139	3.48	0.54	0.000	32 28 4	Right Anterior Insula
		3.06		0.001	32 22 −4	Right Anterior Insula
	5	3.11	0.47	0.001	−36 −10 22	Left Middle Insula

Contrasts without significant correlations are not listed. Z values are for peaks, r^2 is for the entire cluster.

Table 3

Significant correlations between differential skin conductance responses and resting metabolism

cluster p(FWE-cor)	cluster size (voxels)	Z	r^2	peak p(unc)	MNI x,y,z	Peak region
Whole brain						
Negative correlations						
0.012	383	4.44	0.71	0.000	2 −54 −50	Right Cerebellum Posterior Lobe
		3.66		0.000	−6 −44 −52	Left Cerebellum Posterior Lobe
		3.29		0.000	−2 −36 −40	Left Cerebellum Posterior Lobe
0.001	634	4.11	0.64	0.000	−36 −56 −44	Left Cerebellum Posterior Lobe
		4.1		0.000	−30 −70 −40	Left Cerebellum Posterior Lobe
Fear network ROIs						
Positive correlations						
	14	2.99	0.44	0.001	12 30 18	Right Dorsal Anterior Cingulate
Negative correlations						
	111	3.06	0.46	0.001	0 −30 −18	Midbrain

Contrasts with no significant correlations are not listed. Z values are for peaks, r^2 is for the entire cluster.

Table 4a

Midbrain metabolism correlates to differential BOLD

cluster p(FWE-cor)	cluster size (voxels)	Z	r^2	peak p(unc)	MNI x,y,z	Peak region
Whole brain	no significant positive o negative correlation clusters					
Fear network ROIs						
Positive correlations	no significant clusters					
Negative correlations	8	2.77	0.38	0.003	0 −14 −12	L. midbrain

Table 4b

dACC metabolism correlates to differential BOLD

cluster p(FWE-cor)	cluster size (voxels)	Z	r^2	peak p(unc)	MNI x,y,z	Peak region
Whole brain						
Positive correlations						
0.001	365	4.74	0.64	0.000	−26 −52 −2	L. Parahipp. Gyrus
		3.86		0.000	−38 −38 −22	L. Fusiform Gyrus
		3.68		0.000	−36 −48 −24	L. Cerebellum Culmen
0.002	332	4.64	0.55	0.000	−34 −78 20	L. Sup. Occipital Gyrus
		3.71		0.000	−24 −70 28	L. Precuneus
		3.68		0.000	−22 −82 32	L. Cuneus
0.006	283	4.39	0.57	0.000	−22 −58 50	L. Precuneus
		3.89		0.000	−20 −50 54	L. Sub-Gyral
		3.12		0.001	−20 −52 40	L. Precuneus
0.043	183	4.06	0.54	0.000	−42 −74 −12	L. Inf. Occip. Gyrus
		3.5		0.000	−48 −64 −12	L. Mid. Occip. Gyrus
0.036	192	4.02	0.59	0.000	26 −74 36	R. Precuneus
		3.65		0.000	22 −72 44	R. Precuneus
0.029	202	3.78	0.54	0.000	14 −50 58	R. Precuneus
		3.65		0.000	6 −54 50	R. Precuneus
		3.35		0.000	16 −60 60	R. Sup. Parietal Lobule
Negative correlations	no significant clusters					
Fear network ROIs						
Positive correlations						
	6	2.86	0.37	0.002	10 −18 −6	R. midbrain
	9	2.72	0.36	0.003	−10 −18 −8	L. midbrain
Negative correlations	no significant clusters					

Table 4c

Anterior insula metabolism correlates to differential BOLD

cluster p(FWE-cor)	cluster size (voxels)	Z	r^2	peak p(unc)	MNI x,y,z	Peak region
Whole brain	no significant positive o negative correlation clusters					
Fear network ROIs						
Positive correlations	no significant clusters					
Negative correlations						
	5	3.52	0.44	0.000	2 20 −10	R. Subgenual ACC
	5	2.93	0.37	0.002	40 6 12	R. Middle Insula

Table 4d

Amygdala metabolism correlates to differential BOLD

cluster p(FWE-cor)	cluster size (voxels)	Z	r^2	peak p(unc)	MNI x,y,z	Peak region
Whole brain	no significant positive o negative correlation clusters					
Fear network ROIs						
Positive correlations	no significant clusters					
Negative correlations						
	7	2.89	0.37	0.002	−30 30 8	L. Anterior Insula

L. Left, R. Right, Inf. Inferior, Mid. Middle, Sup, Superior, Parahipp Parahippocampal, Occip Occippital, ACC Anteior Cingulate Cortex